Yanbu Journal of Engineering and Science

Volume 22 | Issue 1 Article 7

2025

Enhanced Photocatalytic Performance of Systematically Designed g-C_3N_4/rGO/TiO_2 Ternary Nanocomposite

Khalid Alshammari
Mechanical Engineering, Jubail Industrial College, Royal Commission for Jubail and Yanbu, Saudi Arabia, shammari_kd@rcjy.edu.sa

Sameer Alghanmi
Mechanical Engineering, Jubail Industrial College, Royal Commission for Jubail and Yanbu, Saudi Arabia

Follow this and additional works at: https://yjes.researchcommons.org/yjes
The journal in which this article appears is hosted on Digital Commons, an Elsevier platform.

Recommended Citation
Alshammari, Khalid and Alghanmi, Sameer (2025), Enhanced Photocatalytic Performance of Systematically Designed g-C_3N_4/rGO/TiO_2 Ternary Nanocomposite, *Yanbu Journal of Engineering and Science*: Vol. 22: Iss. 1, 76-83.
DOI: https://doi.org/10.53370/1658-5321.1195
Available at: https://yjes.researchcommons.org/yjes/vol22/iss1/7

This Research Article is brought to you for free and open access by Yanbu Journal of Engineering and Science. It has been accepted for inclusion in Yanbu Journal of Engineering and Science by an authorized editor of Yanbu Journal of Engineering and Science.

YANBU JOURNAL OF ENGINEERING AND SCIENCE 2025;22:76–83

Scan the QR to view the full-text article on the journal website

RESEARCH ARTICLE

Enhanced Photocatalytic Performance of Systematically Designed g-C_3N_4/rGO/TiO_2 Ternary Nanocomposite

Khalid Alshammari *, Sameer Alghanmi

Mechanical Engineering, Jubail Industrial College, Royal Commission for Jubail and Yanbu, Saudi Arabia

ABSTRACT

Graphitic carbon nitride (g-C_3N_4) has become a favorable photocatalyst due to its unique optoelectronic properties, however high recombination rate and low separation efficiency of the photogenerated charge carriers restrict their practical usage. To minimize the recombination rate, we synthesized a ternary nanocomposite, g-C_3N_4/rGO/TiO_2 via a facile, simple, and cost-effective mechanochemistry technique. The ternary nanocomposite effectively degrades Rhodamine B (RhB) dye mainly due to higher visible light utilization and multi-step charge transfer mechanism. The optimal rGO plays an essential role in effective photocatalytic performance due to its unique electrical, large surface area, and optical properties. The synthesized nanocomposite degrades 80 % RhB dye compared to pristine g-C_3N_4 and binary which degrades 39.6 and 64.8 % respectively in 2h. This study showcases a simple, low-cost method for the effective degradation of dyes.

Keywords: Ternary heterojunction photocatalyst, Visible light utilization, RhB dye degradation

1. Introduction

The demand for renewable energy and environmental pollution rate is increasing due to continuous growth in the world population. Semiconductor photocatalysts have fascinated great concern due to their unique properties like degradation of pollutants, converting carbon dioxide into hydrocarbons, self-cleaning surfaces, and renewable energy (H_2) from water splitting, etc [1–3]. Titanium dioxide TiO_2 has received significant attention as a result of its advantages like high chemical inertness, cost-effectiveness, rational photocatalytic activity, environmental safety, and high availability [4]. However, TiO_2 possesses a wide bandgap which restricts its application in the visible light region [5]. To enhance the photocatalytic performance of TiO_2 several modification techniques like element doping [6], fabricating micro-/nano-heterostructures [7], integrating with other visible-light semiconductors [8], and nanocarbon [9], are frequently used.

Graphitic carbon nitride (g-C_3N_4) has acquired noticeable attraction due to its appropriate bandgap of approximately 2.7 eV, large surface area, and nontoxicity making it potentially useful for water splitting (H_2) production [10], environmental purification [11], and CO_2 reduction [12]. However, pristine g-C_3N_4 demonstrates a high photogenerated carrier recombination rate as well as a low specific surface area which limits its practical application [13, 14].

To enhance the efficiency of g-C_3N_4 several modification techniques are utilized such as metal or nonmetal deposition, Z-scheme junctions, and semiconductor assembly/type-II heterojunction schemes, [15, 16]. Compared to other types, II heterojunction methods provide a facile route for the effective separation and transport of photogenerated charge carriers [16]. In this scheme, g-C_3N_4 were assembled

Received 24 September 2024; revised 20 November 2024; accepted 14 December 2024.
Available online 1 June 2025

* Corresponding author.
E-mail address: shammari_kd@rcjy.edu.sa (K. Alshammari).

https://doi.org/10.53370/1658-5321.1195
1658-5321/© 2025 The Author(s). Yanbu Journal of Engineering and Science. This is an open access article under the CC BY 4.0 Licence (https://creativecommons.org/licenses/by/4.0/).
Published by Yanbu Industrial College, Saudi Arabia. The journal is hosted on Digital Commons, an Elsevier Platform.

with semiconductors having conduction bands (CB) lower than g-C_3N_4 while valence band (VB) higher than g-C_3N_4 to effectively separate the photogenerated charge carriers [17]. For example, Madima and Zhang *et al.,* synthesized g-C_3N_4/TiO_2 nanocomposite performing effective photocatalytic performance compared to pristine g-C_3N_4 [18, 19]. However, type-II heterojunction methods demonstrate some disadvantages too, such as lacking visible-light utilization, quick charge recombination, and slow surface redox kinetics [20]. To enhance the photocatalytic performance of binary heterojunction, one of the facile techniques is the introduction of 2D conductive graphene oxide (GO) and/or reduced graphene oxide (rGO) into binary heterojunction due to its unique electrical and optical properties, and large surface area [21, 22]. rGO insertion in binary composite enhances specific surface area, creating new electron-transfer paths, and boosting the surface adsorption and reaction kinetics, thus accomplishing the enhanced photocatalytic performance [21, 23]. Wu and Khan *et al.* synthesized ternary nanocomposite utilizing a hydrothermal technique demonstrating effective dye degradation performance compared to binary heterojunction [20, 24].

In this work, a mechanochemistry method was employed to synthesize g-C_3N_4/rGO/TiO_2 ternary heterojunction photocatalyst. The synthesized photocatalyst with optimized rGO content demonstrates enhanced photocatalytic performance mainly due to higher visible light utilization and multi-step charge transfer mechanism. The synthesized nanocomposite degrades 80 % RhB dye compared to pristine g-C_3N_4 and binary which degrades 39.6 and 64.8 % respectively in 2h. The structural, morphological, optical, and charge-separation features of ternary heterojunctions were studied in-depth by utilizing various techniques.

2. Experimental section

2.1. Materials and chemicals used

All metal-based salts were purchased from Sigma Aldrich, while laboratory-grade chemicals like graphite powder and solvents such as acid, methanol, deionized water, etc., were obtained from Jubail, KSA. All the chemicals utilized in the experimentation were of analytical grade and were utilized without any further purification.

2.2. Synthesis of g-C_3N_4/rGO/TiO_2 ternary nanocomposite

Graphene oxide (GO) was synthesized via the modified Hummers method [25]. Take 25 mL of H_2SO_4 in a beaker, then add 1 g of graphite powder and 0.5 g of $NaNO_3$. Next, add 3 g of $KMnO_4$ to the above solution, stirring continuously while maintaining the temperature at 40 ˚C using an ice bath for 12 hours. As a result of this procedure, brown GO (graphene oxide) was obtained, which was washed several times and finally dried in an oven at 60 ˚C for 10 hours. Hou *et al.,* [26], utilized both pristine g-C_3N_4 and g-C_3N_4/rGO nanocomposite. For pristine, first g-C_3N_4 only urea was utilized while for g-C_3N_4/rGO nanocomposite preparation, first dissolve 7 mg powder of GO in 40 mL of water by ultrasonic treatment for 300 mins. Add 20 g urea under stirring followed by heating at 65 ˚C. The GO/urea products were then transferred to a furnace, maintaining the temperature at 550 ˚C for 4 h resulting in g-C_3N_4/rGO. To synthesize ternary nanocomposite we take 0.4 mL of ethanol, agate balls, specific amounts of g-C_3N_4/rGO and TiO_2 in an agate jar. The blends were ball-milled at 400 rpm for 5 h using a XQM-0.4 planetary ball mill (TENCAN). The product was then dried at 60 ˚C for 12 h. We applied the same method by combining different g-C_3N_4, rGO and TiO_2 ratio/percentage, such as (75% g-C_3N_4, 2% rGO and 23% TiO_2), (75% g-C_3N_4, 5% rGO and 20% TiO_2) and (75% g-C_3N_4, 10% rGO and 15% TiO_2) among different ratio/percentage 75%/g-C_3N_4/5% rGO/20% TiO_2 nanocomposite effectively perform dye degradation performance.

2.3. Characterization

X-ray diffractometer (D/Max-2500/PC, Rigaku) was utilized to evaluate the crystallinity and phase purity of all the samples. Morphological and structural details were studied utilizing scanning electron microscopy (FESEM, HITACHI, S4800). Crystallographic structures were studied using transmission electron microscopy (HRTEM, JEOL, JEM2100F). FT-IR spectrometer (Thermo Fisher Scientific, NICOLET iS10) was utilized to find the functional groups and bending vibration. Electrochemical impedance spectra were obtained using (CHI 760 D, CH Instruments) in a frequency range of 100 Hz - 1 MHz. UV–vis spectrophotometer (JASCO, V650) was utilized to evaluate the absorbance behavior.

2.4. Photocatalysis

Photocatalytic activity evaluation was assessed by the degradation of Rhodamine B (RhB) dye [21]. A concentration of 0.0072 g/L of RhB dye was the optimal recipe to prepare the standard solution [27]. To evaluate the photocatalytic performance, 0.03 g of each sample was dispersed in 200 mL of the RhB aqueous solution, followed by sonication and stirring

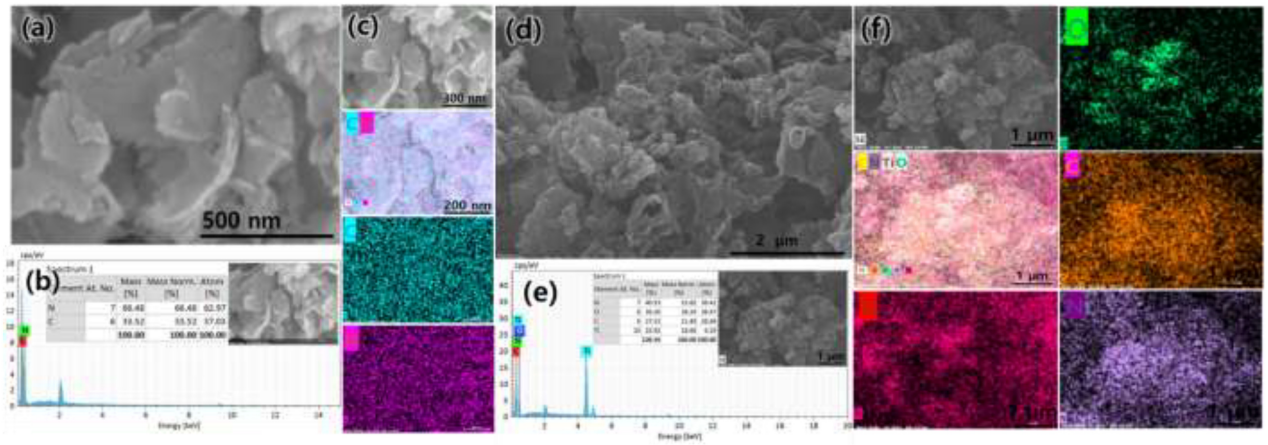

Fig. 1. (a) SEM, (b) EDS, (c) area mapping of prsitne g-C_3N_4 (d) SEM, (e) EDS, and (f) area mapping of ternary nanocomposite.

to uniformly distribute the powder within the solution. Subsequently, solution was kept in light irradiation for 120 mins utilizing halogen lamp equipped with UV-absorbing glass filter (HI-Spot 95), (100W, $\lambda > 420$ nm) manufactured by Osram Sylvania Inc. Luminous intensity was found to be 80 klux (~11.7 mW cm^{-2} or 7400 foot-candle), measured by a lux meter (TES-1339 Light Meter Pro) at numerous points.

3. Results and discussion

SEM measurements were done to study the morphology of the pristine g-C_3N_4 as well as the nanocomposite. Pristine g-C_3N_4 possesses a layer-type structure as shown in Fig. 1(a). Additionally, Fig. 1(d), demonstrates SEM images of ternary nanocomposite which demonstrate the existence of both g-C_3N_4 and TiO_2 particles. EDS measurements were done both for pristine as well as ternary to evaluate the presence of each element along with its atomic ratios as revealed in Fig. 1(b & e). Moreover, elemental area mapping was done both for pristine as well as ternary to evaluate the uniform distribution of each element in nanocomposite as revealed in Fig. 1(c & f).

Additionally, TEM analysis was done to evaluate in depth the crystallographic structure as shown in Fig. 2(a–c). Distinct lattice fringes of 0.351 and 0.31 nm demonstrate (101) and (002) planes of TiO_2, and g-C_3N_4 along with the presence of rGO at such a high magnification confirming the formation of close junction which became the reason for effective charge separation as well migration. As revealed in Fig. 2c selected-area electron diffraction (SAED) correspondingly demonstrates different TiO_2 planes.

Additionally, the crystallinity of g-C_3N_4, binary, and ternary nanocomposite was evaluated via XRD analysis as shown in Fig. 3. Pristine g-C_3N_4 demonstrates two diffraction peaks at 13.1° and 27.4° are consistent with previous literature [17, 28]. The peak positions at 25.3°, 37.9°, and 48.0° correspond to the (101), (004), and (200) planes of TiO_2 for both the binary and ternary nanocomposites [29, 30]. Moreover, the peaks of TiO_2 and g-C_3N_4 observed in both the binary and ternary graphs demonstrate the successful formation of the nanocomposite. Furthermore, the XRD pattern of pristine TiO_2 and rGO demonstrates the corresponding diffraction peaks as shown in Fig. S1.

To evaluate the attachment of functional groups with synthesized materials FTIR analysis was

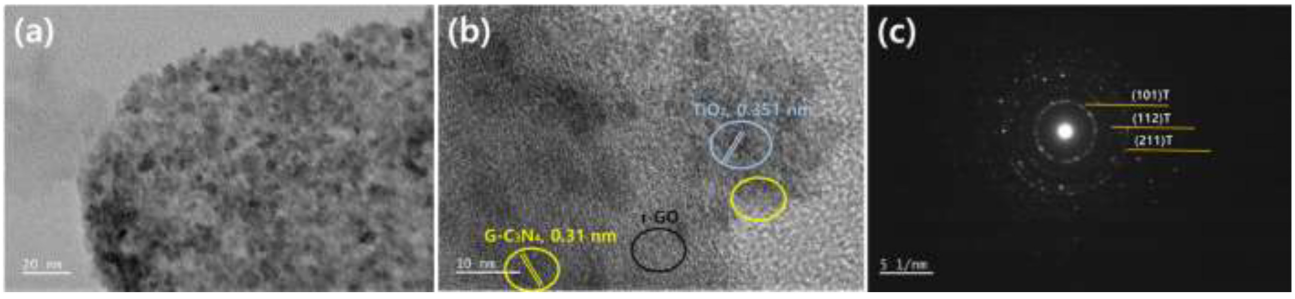

Fig. 2. (a) Low, (b) high amplification HRTEM images, and (i) SAED pattern ternary nanocomposite.

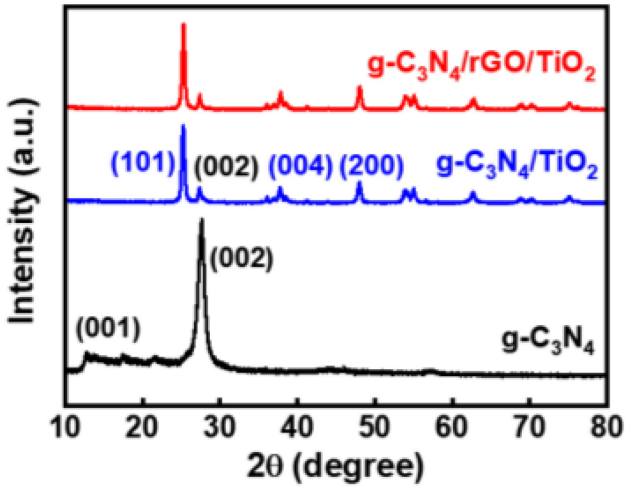

Fig. 3. XRD patterns of ternary nanocomposite.

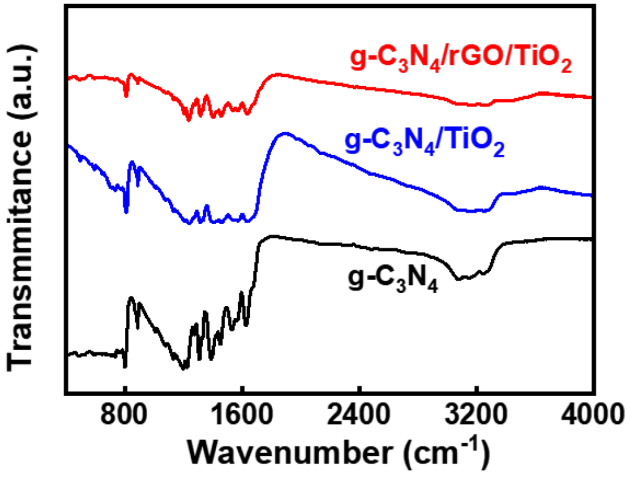

Fig. 4. FTIR spectra.

performed as revealed in Fig. 4. Pristine, binary, and ternary nanocomposite demonstrate the peak at ~805 cm^{-1} allocated to triazine units indicating that during nanocomposite formation the morphology of g-C_3N_4 remains unaffected [27]. Additionally, in all synthesized materials the absorption bands from ~1250–1750 cm^{-1} represent the C =N, C–N bond [14, 15, 31]. Additionally, the peak at ~3000–3400 cm^{-1} allocated to OH stretching and NH overlying mode [32]. Furthermore, (Fig. S2) demonstrate vibration mode of pristine TiO_2.

Additionally, the absorbance behavior of all samples was evaluated via UV-vis spectra as revealed in Fig. 5(a–b). $\alpha h\nu = A\ (h\nu - E_g)^{n/2}$ equation was used to evaluate the corresponding (E_g) values. The (E_g) were calculated by $(\alpha h\nu)^{1/2}$ versus ($h\nu$) giving nearly 2.63, 2.65, and 2,56 eV [33] as revealed in Fig. 5b. Compared to pure g-C_3N_4 synthesized ternary nanocomposite demonstrates redshift, due to rGO insertion [34]. These results demonstrate that enhanced photon absorption takes place in ternary nanocomposite which in turn produces a greater number of photogenerated charge carriers which are essential for dye degradation.

EIS analysis (Fig. 6) was used to evaluate the separation, migration, and recombination behavior of synthesized photocatalysts. The EIS analysis is exactly related to recombination resistance (R_{rec}), series resistance (R_s), and junction capacitance of the devices (Fig. S3) as well as Table S1 demonstrates the extracted values. R_{rec} value is directly related to the diameter of semicircle [35] [27]. Compared to pristine as well as binary nanocomposite, synthesized ternary nanocomposite demonstrates a smaller R_{rec}

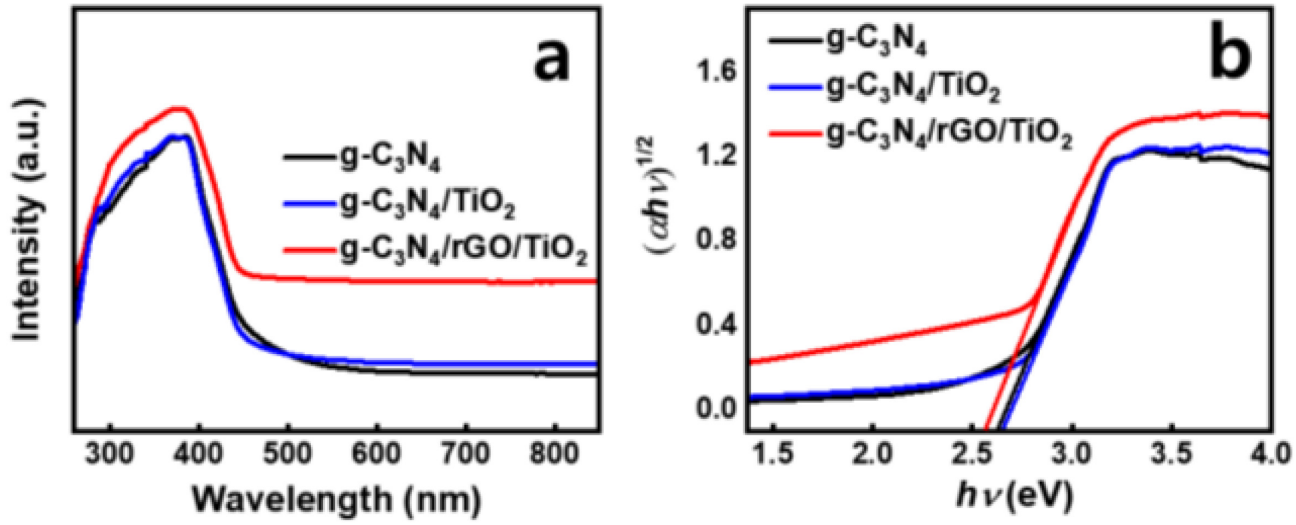

Fig. 5. (a) Visible absorption, and (b) Corresponding band gap.

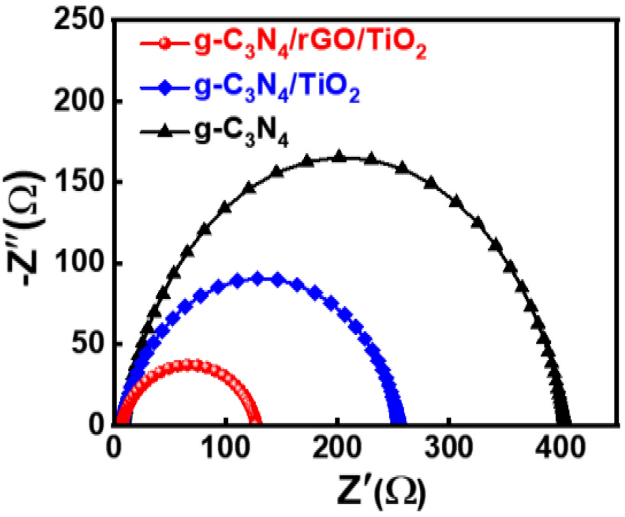

Fig. 6. Nyquist plots of all the synthesized nanocomposite.

value responsible for effective charge separation and transfer, resulting in active RhB dye degradation.

Photocatalytic activity of pristine as well as nanocomposite was plotted as C/C_0 vs t where (where C_0 represents initial concentration and C as the concentration of dye after irradiation time), under visible light as shown in Fig. 7 as well as Fig. S4. With time, a significant decrease in dye concentration can be seen as shown in Fig. 7a. Furthermore, ternary nanocomposite (Fig. 7b) demonstrates higher (Kc) compared to pristine as well as binary nanocomposite which indicates higher forward reaction [36]. From dye concentration and Kc values, it is clear that the photocatalyst synthesized via the mechanochemistry method degraded 80% RhB dye in 2 h due to effective charge separation as well as transfer. Specific chemicals such as BQ, EDTA-2Na, and IPA, were added to the solution as scavengers aimed at $^{\bullet}O_{2^-}$, H^+, and $^{\bullet}OH$, respectively in the dye-degradation process [37].

Fig. S5 demonstrates that BQ and AO addition to the solution-suppressed dye degradation process suggested that $^{\bullet}O_2^-$ and H^+ are the main reacting species. Moreover, IPA addition slightly affects dye degradation indicating that $^{\bullet}OH$ plays a minor role in the photodegradation process.

From the preceding discussion and results a schematic was constructed which illustrates the generation, separation, and transfer of photogenerated charge as shown in Fig. 8. Since the CB position of g-C_3N_4 (−1.12V vs. NHE) is higher than TiO_2 (−0.5V vs. NHE) which in turn is higher than rGO (−0.08V vs. NHE) [24]. When visible light strikes the ternary nanocomposite photogenerated electron moves from CB of g-C_3N_4 toward TiO_2 and finally to rGO via a multi-step electron transfer mechanism which is feasible both electrically and thermodynamically. The rGO performs both the role of transferring and shuttling at the TiO_2/g-C_3N_4 interface. Additionally, rGO performed both the function of shuttling and co-catalyst due to its lower band gap position compared to TiO_2 and g-C_3N_4, O_2 quickly transfers from CB of TiO_2 to rGO, producing $^{\bullet}O_2$ radicals which is crucial for dye degradation [16, 38–40]. These $^{\bullet}O_2^-$ radicals play a crucial role in dye degradation. Furthermore, H^+ at VB of g-C_3N_4 having higher oxidation potential directly oxidizes the RhB dye molecules. Efficient dye degradation takes place due to effective generation, separation, and transfer of photogenerated charge in

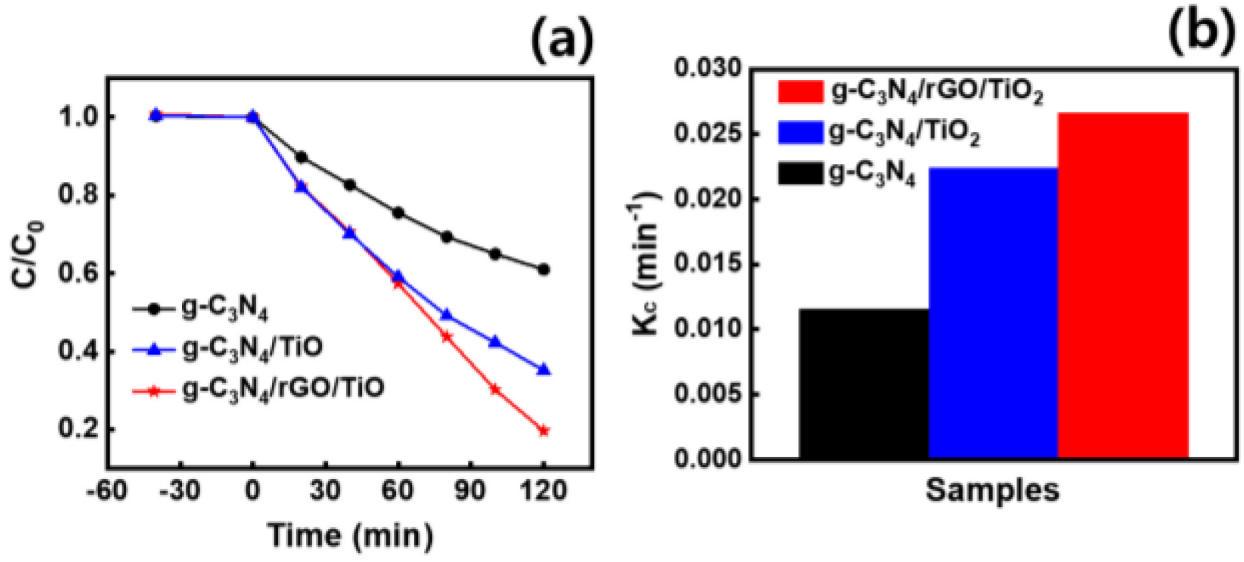

Fig. 7. (a) Dye degradation under visible light and (b) Reaction rate constants i.e. Kc.

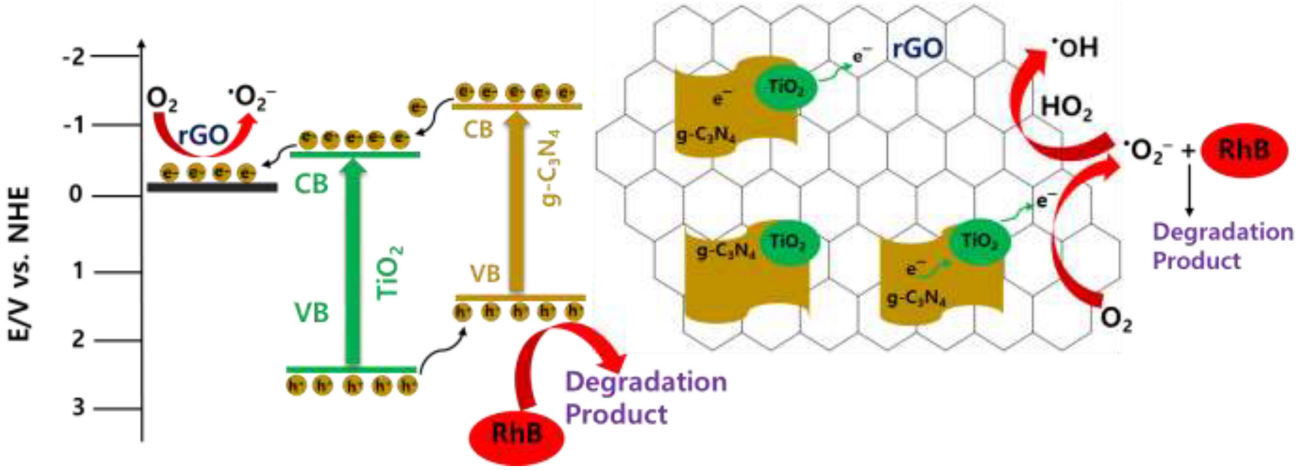

Fig. 8. Schematic diagram demonstrates charge separation and transfer in ternary nanocomposite for dye degradation under visible irradiation.

nano/heterojunction photocatalysts. The procedure for improved photocatalytic activity of nanocomposite can be briefed as [41]:

$$g\text{-}C_3N_4 + TiO_2 + rGO + hv \rightarrow g\text{-}C_3N_4(H^+) + TiO_2(e^-) + rGO(e^-) \quad (1)$$

$$rGO(e^-) + O_2 \rightarrow rGO + {}^{\bullet}O_{2^-} \quad (2)$$

$${}^{\bullet}O_{2^-}/g\text{-}C_3N_4(H^+) + RhB \rightarrow \text{degradation products} \quad (3)$$

Stability of the synthesized nanocomposite was done to evaluate its practical application as shown in Fig. 9. Even after 5 successive cycles, a slight change in the photocatalytic activity was seen. We recovered the amount of each sample used in the experiment through the centrifuge process. After five successive experiments, the recovered samples were weighed using a balance, amounting to 0.027 g.

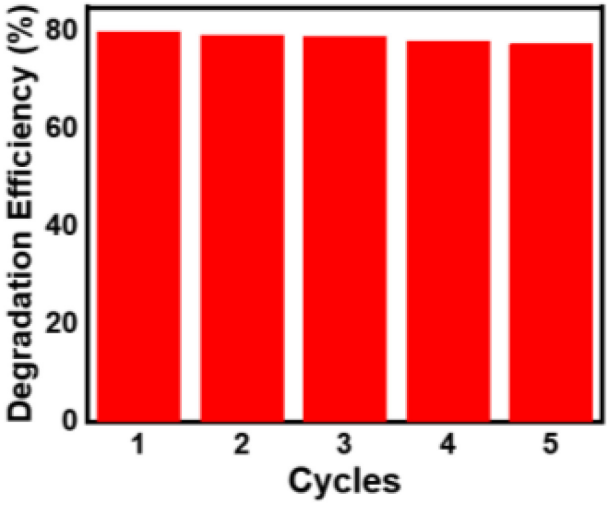

Fig. 9. Stability test of photocatalyst using RhB dye.

4. Conclusion

In summary, ternary g-C_3N_4/rGO/TiO_2 nanocomposite was synthesized via a mechanochemistry method demonstrating effective photocatalytic performance as well as stability. The ternary nanocomposite effectively degrades Rhodamine B (RhB) dye mainly due to higher visible light utilization and multi-step charge transfer mechanism. The optimum rGO plays both the role of transferring and shuttling at the TiO_2/g-C_3N_4 interface. This work presents and opens the way for effective dye degradation and environment purification applications utilizing a facile, and cost-effective technique.

Conflict of interest

The authors declare no conflict of interest.

Author contribution

Khalid Alshammari was responsible for writing the manuscript, visualization, and software analysis. Sameer Alghanmi reviewed the paper, supervised the work, and participated in the analysis.

Data availability

The authors confirm that the data supporting the findings of this study are available within the article [and/or] its supplementary materials.

References

1. Jiang X, Wang P, J. Zhao. 2D covalent triazine framework: a new class of organic photocatalyst for water splitting. *J. Mater. Chem. A*. Mar. 2015;3(15):7750–8, doi: 10.1039/C4TA03438D.
2. Zhang S, *et al.* In situ synthesis of water-soluble magnetic graphitic carbon nitride photocatalyst and its synergistic catalytic performance. *ACS Appl Mater Interfaces*. Dec. 2013;5(23):12735–43, doi: 10.1021/am404123z.
3. Schultz DM, Yoon TP. Solar synthesis: prospects in visible light photocatalysis. *Science*. Feb. 2014;343(6174):1239176, doi: 10.1126/science.1239176.
4. Wen J, Li X, Liu W, Fang Y, Xie J, Y. Xu. "Photocatalysis fundamentals and surface modification of TiO2 nanomaterials. *Chinese Journal of Catalysis*. 2015;12(36):2049–70, doi: 10.1016/S1872-2067(15)60999-8.
5. Li X, Yu J, Low J, Fang Y, Xiao J, X. Chen. Engineering heterogeneous semiconductors for solar water splitting. *J. Mater. Chem. A*. Jan. 2015;3(6):2485–534, doi: 10.1039/C4TA04461D.
6. M. S. Akple *et al.* Nitrogen-doped TiO2 microsheets with enhanced visible light photocatalytic activity for CO2 reduction. *Chinese Journal of Catalysis*. 2015;12(36):2127–34, doi: 10.1016/S1872-2067(15)60989-5.
7. Li X, Yu J, M. Jaroniec. Hierarchical photocatalysts. *Chem. Soc. Rev.* May 2016;45(9):2603–36, doi: 10.1039/C5CS00838G.
8. Papailias I, Todorova N, Giannakopoulou T, Yu J, Dimotikali D, Trapalis C. Photocatalytic activity of modified g-C3N4/TiO2 nanocomposites for NOx removal. *Catalysis Today*. Feb. 2017;280:37–44, doi: 10.1016/j.cattod.2016.06.032.
9. Low J, Yu J, W. Ho. Graphene-Based Photocatalysts for CO2 Reduction to Solar Fuel. *J. Phys. Chem. Lett.* Nov. 2015;6(21):4244–51, doi: 10.1021/acs.jpclett.5b01610.
10. Akple MS, Low J, Wageh S, Al-Ghamdi A. A, Yu J, J. Zhang. Enhanced visible light photocatalytic H2-production of g-C3N4/WS2 composite heterostructures. *Applied Surface Science*. 2015;PartA(358):196–203, doi: 10.1016/j.apsusc.2015.08.250.
11. L. Pi, *et al.* g-C3N4 Modified biochar as an adsorptive and photocatalytic material for decontamination of aqueous organic pollutants. *Applied Surface Science*. Dec. 2015;358:231–9, doi: 10.1016/j.apsusc.2015.08.176.
12. Cao S, Low J, Yu J, M. Jaroniec. Polymeric Photocatalysts based on graphitic carbon nitride. *Advanced Materials*. 2015;27(13):2150–76, doi: 10.1002/adma.201500033.
13. Niu P, Zhang L, Liu G, Cheng H.-M. Graphene-Like carbon nitride nanosheets for improved photocatalytic activities. *Advanced Functional Materials*. 2012;22(22):4763–70, doi: 10.1002/adfm.201200922.
14. Ali G, Jazib Abbas Zaidi S, Abdul Basit M and Park TJ. Synergetic performance of systematically designed g-C3N4/rGO/SnO2 nanocomposite for photodegradation of Rhodamine-B dye. *Applied Surface Science*. Dec. 2021;570:151140, doi: 10.1016/j.apsusc.2021.151140.
15. Zhao Z, Sun Y, and F. Dong. Graphitic carbon nitride based nanocomposites: a review. *Nanoscale*. Dec. 2014;7(1):15–37, doi: 10.1039/C4NR03008G.
16. Low J, Yu J, Jaroniec M, Wageh S, Al-Ghamdi A. A. Heterojunction Photocatalysts. *Advanced Materials*. 2017;29(20):1601694, doi: 10.1002/adma.201601694.
17. X. Chen *et al.* In situ construction of an SnO2/g-C3N4 heterojunction for enhanced visible-light photocatalytic activity. *RSC Adv*. Aug. 2015;5(84):68953–63, doi: 10.1039/C5RA11801H.
18. Madima N, Kefeni KK, Mishra SB, and Mishra AK. TiO2-modified g-C3N4 nanocomposite for photocatalytic degradation of organic dyes in aqueous solution. *Heliyon*. Sep. 2022;8(9):e10683, doi: 10.1016/j.heliyon.2022.e10683.
19. X. Zhang and Jiang SP. Layered g-C3N4/TiO2 nanocomposites for efficient photocatalytic water splitting and CO2 reduction: a review. *Materials Today Energy*. Jan. 2022;23:100904, doi: 10.1016/j.mtener.2021.100904.
20. M. Khan, *et al.* Improved electro- and photo-catalytic performance of simplistically developed g-C3N4/rGO/TiO2 nanocomposite. *Journal of Photochemistry and Photobiology A: Chemistry*. Nov. 2024;456:115820, doi: 10.1016/j.jphotochem.2024.115820.
21. Iwase A, Ng YH, Ishiguro Y, Kudo A, and Amal R. Reduced graphene oxide as a solid-state electron mediator in Z-scheme photocatalytic water splitting under visible light. *J Am Chem Soc*. Jul. 2011;133(29):11054–7, doi: 10.1021/ja203296z.
22. Iwase A, Yoshino S, Takayama T, Ng YH, Amal R, and Kudo A. Water Splitting and CO2 Reduction under Visible Light Irradiation Using Z-Scheme Systems Consisting of Metal Sulfides, CoOx-Loaded BiVO4, and a Reduced Graphene Oxide Electron Mediator. *J. Am. Chem. Soc.* Aug. 2016;138(32):10260–4, doi: 10.1021/jacs.6b05304.
23. Li Q, Li X, Wageh S, Al-Ghamdi Ahmed A, Yu J. CdS/Graphene nanocomposite photocatalysts. *Advanced Energy Materials*. 2015;5(14):1500010, doi: 10.1002/aenm.201500010.
24. Wu F, Li X, Liu W, S. Zhang. Highly enhanced photocatalytic degradation of methylene blue over the indirect all-solid-state Z-scheme g-C3N4-RGO-TiO2 nanoheterojunctions. *Applied Surface Science*. 2017;405(Complete):60–70, doi: 10.1016/j.apsusc.2017.01.285.
25. W. S. Jr. Hummers Offeman RE. Preparation of graphitic oxide. *J. Am. Chem. Soc.* Mar. 1958;80(6):1339–9, doi: 10.1021/ja01539a017.
26. Hou Y, Wen Z, Cui S, Guo X, J. Chen. Constructing 2D Porous Graphitic C3N4 Nanosheets/Nitrogen-Doped Graphene/Layered MoS2 Ternary Nanojunction with Enhanced Photoelectrochemical Activity. *Advanced Materials*. 2013;25(43):6291–7, doi: 10.1002/adma.201303116.
27. J. Khan, *et al.* Quantum-dot sensitized hierarchical NiO p–n heterojunction for effective photocatalytic performance. *RSC Adv*. Nov. 2022;12(50):32459–70, doi: 10.1039/D2RA05657G.
28. Dai K, Lu L, Liang C, Liu Q, Zhu G. Heterojunction of facet coupled g-C3N4/surface-fluorinated TiO2 nanosheets for organic pollutants degradation under visible LED light irradiation. *Applied Catalysis B: Environmental*. Sep. 2014;156–157:331–40, doi: 10.1016/j.apcatb.2014.03.039.
29. Ali G, Ali I, Ali Marwat M, J Khan, Basit M. Abdul, Park T. Joo. Template-free hierarchical TiO2/rGO nanocomposites for enhanced photocatalytic performance. *Chemical Physics Letters*. Aug. 2024;848:141372, doi: 10.1016/j.cplett.2024.141372.
30. Malik A, Muhyuddin M, Ali G, Wadood A, Tauqir A, Basit MA. Bi-efficacious incorporation of Indium in TiO2/PbS based nanocomposites for photocatalytic and solar paint applications. *Solar Energy*. Nov. 2021;228:216–25, doi: 10.1016/j.solener.2021.09.057.
31. Yang Y, Chen J, Mao Z, An N, Wang D, Fahlman BD. Ultrathin g-C3N4 nanosheets with an extended visible-light-responsive range for significant enhancement of photocatalysis. *RSC Adv*. Jan. 2017;7(4):2333–41, doi: 10.1039/C6RA26172H.
32. Gu L, Wang J, Zou Z, Han X. Graphitic-C3N4-hybridized TiO2 nanosheets with reactive {0 0 1} facets to enhance the UV- and visible-light photocatalytic activity. *Journal of Hazardous*

Materials. Mar. 2014;268:216–23, doi: 10.1016/j.jhazmat.2014.01.021.
33. G. Bi, *et al.* Efficient visible-light photocatalytic H2 evolution over metal-free g-C3N4 co-modified with robust acetylene black and Ni(OH)2 as dual co-catalysts. *RSC Adv*. Mar. 2016;6(37):31497–506, doi: 10.1039/C6RA03118H.
34. T.-F. Yeh, J.-M. Syu, Cheng C, Chang T.-H, H. Teng. Graphite Oxide as a Photocatalyst for Hydrogen Production from Water. *Advanced Functional Materials*. 2010;20(14):2255–62, doi: 10.1002/adfm.201000274.
35. Braga A, Giménez S, Concina I, Vomiero A, I. Mora-Seró. Panchromatic Sensitized Solar Cells Based on Metal Sulfide Quantum Dots Grown Directly on Nanostructured TiO2 Electrodes. *J. Phys. Chem. Lett.* Mar. 2011;2(5):454–60, doi: 10.1021/jz2000112.
36. Wu F, Li X, Liu W, S. Zhang. Highly enhanced photocatalytic degradation of methylene blue over the indirect all-solid-state Z-scheme g-C3N4-RGO-TiO2 nanoheterojunctions. *Applied Surface Science*. May 2017;405:60–70, doi: 10.1016/j.apsusc.2017.01.285.
37. Hu L, Chen F, Hu P, Zou L, Hu X. Hydrothermal synthesis of SnO2/ZnS nanocomposite as a photocatalyst for degradation of Rhodamine B under simulated and natural sunlight. *Journal of Molecular Catalysis A: Chemical*. Jan. 2016;411:203–13, doi: 10.1016/j.molcata.2015.10.003.
38. Y.-J. Yuan, *et al.* Promoting Charge Separation in g-C3N4/Graphene/MoS2 Photocatalysts by Two-Dimensional Nanojunction for Enhanced Photocatalytic H2 Production. *ACS Applied Energy Materials*. Mar. 2018, doi: 10.1021/acsaem.8b00030.
39. Shi F, Chen L, Xing C, Jiang D, Li D, Chen M. ZnS microsphere/g-C3N4 nanocomposite photo-catalyst with greatly enhanced visible light performance for hydrogen evolution: synthesis and synergistic mechanism study. *RSC Adv*. Nov. 2014;4(107):62223–9, doi: 10.1039/C4RA11740A.
40. Zhang Z, Jiang D, Li D, He M, and Chen M. Construction of SnNb2O6 nanosheet/g-C3N4 nanosheet two-dimensional heterostructures with improved photocatalytic activity: Synergistic effect and mechanism insight. *Applied Catalysis B: Environmental*. Apr. 2016;183:113–23, doi: 10.1016/j.apcatb.2015.10.022.
41. Pawar RC, Khare V, and Lee CS. Hybrid photocatalysts using graphitic carbon nitride/cadmium sulfide/reduced graphene oxide (g-C3N4/CdS/RGO) for superior photodegradation of organic pollutants under UV and visible light. *Dalton Trans*. Jul. 2014;43(33):12514–27, doi: 10.1039/C4DT01278J.